Available online at www.sciencedirect.com
ScienceDirect
Ceramics International 37 (2011) 2829–2835
CERAMICS INTERNATIONAL
www.elsevier.com/locate/ceramint

# Microstructure and frictional properties of C/SiC brake materials with sandwich structure

Shangwu Fan *, Litong Zhang, Laifei Cheng, Shangjie Yang

*National Key Laboratory of Thermostructure Composite Materials, Northwestern Polytechnical University, Xi'an, Shaanxi 710072, China*

Received 15 February 2011; received in revised form 15 April 2011; accepted 27 April 2011
Available online 5 May 2011

**Abstract**

C/SiC brake materials with a sandwich structure were prepared by three step process, chemical vapor infiltration, slurry infiltration and liquid silicon infiltration process. The fabricated brake materials consist of a C-fiber rich main body and two SiC-rich frictional layers on the surface. The microstructure and frictional properties of C/SiC brake materials were investigated. The results indicated that the density and open porosity of the materials were 2.2 g/cm$^3$ and 4%, respectively. The phase distribution in the friction layers of C/SiC with sandwich structure was homogeneous, and the silicon was little and dispersed in the friction functional layers. The joining region between friction functional layer and mechanical functional layer has an inter-laminar shear strength of about 27 ± 9 MPa, indicating its reliability. The frictional properties under wet condition of the C/SiC with the sandwich structure showed no fading, and were better than that of the 3D needled C/SiC. The static friction coefficient and linear wear rate of the C/SiC with the sandwich structure was higher than that of the 3D needled C/SiC. The C/SiC brake materials with sandwich structure would have higher brake efficiency.


*Keywords:* B. Composites; B. Microstructure-final; C. Friction; C/SiC; Brake materials

## 1. Introduction

C/SiC composites are a new type of high performance brake materials developed after the powder metallurgy materials and C/C composites. C/SiC composites exhibit a series of outstanding advantages such as low density, good high temperature resistance, high damage tolerance, excellent friction properties, low wear rate and long life [1–6].

The first development of the C/SiC brake was made by British Engineers working in the railway industry for TGV applications in 1988 [7]. In the early 1990s, Krenkel et al. at the German Aerospace Center (DLR) in Stuttgart started investigations of C/SiC composites for high performance automobile applications [2,3,8]. Up to now, the C/SiC brakes have been successfully applied to Porsche, Ferrari and Daimler Chrysler [9,10]. For automobiles, the abrasion resistance of the C/SiC disks guarantees a service life of 300,000 km which is 4 times greater than that of steel disks [4,10]. In recent years, plenty of work have been done for development of C/SiC aircraft brake materials [1,5,6]. In 2008, the flight test of the C/SiC aircraft brakes was accomplished successfully [11].

As brake materials, good frictional and mechanical properties are necessary. The 3D needled C/SiC brake materials possessed good mechanical properties and excellent braking performance [5,6]. However, its frictional properties are not stable because the phase under a certain depth from the friction surface was inhomogeneous, and the Si was presented clumped distribution in 3D needled C/SiC to induce adhesive wear [12]. In this paper, we report a newly developed aircraft C/SiC brake materials with a sandwich structure composed of two outer functional layers for friction, and inner mechanical functional layer. In the functional layer for friction, homogeneous phase distribution and improved stability of the frictional properties were achieved. The objective of the present study was to investigate the microstructure and frictional properties of C/SiC brake materials with sandwich structure.

* Corresponding author. Tel.: +86 29 8849 4622; fax: +86 29 8849 4620.
*E-mail addresses:* fshwu@163.com, Shangwu_Fan@nwpu.edu.cn (S. Fan).

0272-8842/$36.00 
doi:10.1016/j.ceramint.2011.04.075

## 2. Experiments

### 2.1. Fabrication

Needled integrated felts with sandwich structure (Fig. 1) were used as preform in this study. The density of the preform was about 0.5 g $cm^{-3}$. The carbon fiber was PAN-based carbon fiber (T300, 12K, Toray, Japan). The carbon fiber preform with sandwich structure was fabricated by the three dimension needling method [6]. The carbon fiber preform was composed of needled integrated felts as inner mechanical functional layer, and thick short-cut web as outer frictional functional layers. Preparation of the C/SiC composites involves three steps. The first one was chemical vapor infiltration (CVI) process to manufacture porous C/C composites with sandwich structure (Fig. 2). The temperature for CVI was about 800–1000 °C for 300–700 h. Propylene was used as a precursor and argon as a carrier and diluting gas. The density of the porous C/C composites was about 1.2–1.7 g $cm^{-3}$. The second step was slurry infiltration (SI) process. The slurry was graphite distilled water solution, and the concentration of the solution was about 30 wt%. The pressure of infiltration was 1 MPa. The third step was liquid silicon infiltration (LSI) process (infiltration of the molten silicon into porous C/C composites), producing the final C/SiC composites. The LSI was conducted at the range of 1420–1700 °C for 1–3 h.

### 2.2. Testing methods

The density and open porosity of C/SiC composites were measured by Archimedes' method. The microstructures were observed by light microscopy (OLYMPUS PM-T3) and Scanning Electron Microscopy (HITACHI S-4700).

The inter-laminar shear test (Double-Notch Compression) was conducted on a universal testing machine (Instron 1196). The test methods are according to the ASTM C1292. The fixture and the geometry of specimen for the inter-laminar shear strength test were shown in Fig. 3. The compressional speed was about 0.05 mm/min.

The frictional properties were tested on a disk-on-disk type laboratory scale dynamometer (Fig. 4) referred to [6]. The kinetic energy absorbed by braking was supplied by the inertia wheels, which were driven by a DC motor. The tested specimens acted as both the rotor and the stator. The rotor specimen was attached to the inertial wheel and accelerated to a certain velocity, the braking property test was carried out through the friction between the rotor and stator under a certain braking pressure. Rotating velocity, braking moment, and braking time were recorded by computer. The friction coefficient can be calculated from Eq. (1).

$$M = \mu(r_1 + r_2)\frac{P}{2} \tag{1}$$

where $M$ is the braking moment, $\mu$ the friction coefficient, $P$ the braking pressure, $r_1$ the inner radius, and $r_2$ is the outer radius.

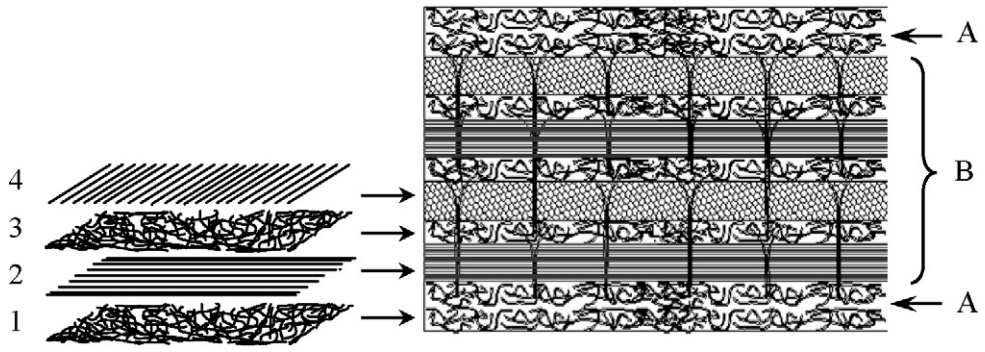


(a) Schematic diagram


(b) Macro photograph

Fig. 1. (a and b) The structure of 3D needled carbon fiber perform with sandwich structure. 1 and 3 were short-cut fiber web, 2 was 0° non-woven fiber cloth, and 4 was 90° non-woven fiber cloth. A was functional layer for friction, and B was mechanical functional layer for load-carrying.

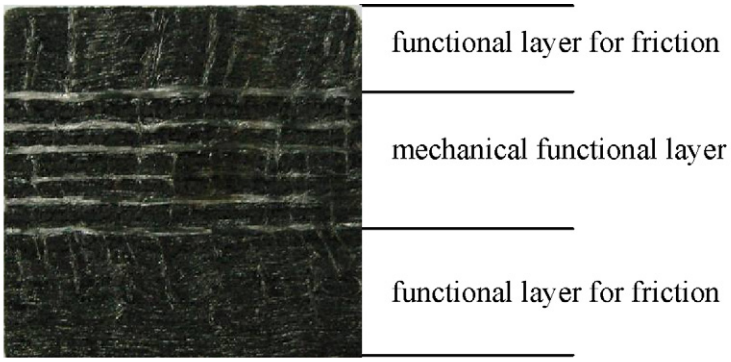


(a) Macro photograph of cross section

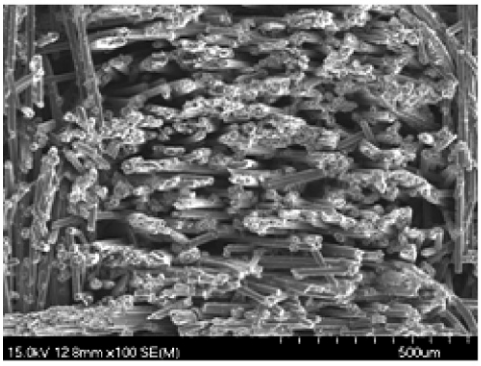

(b) Functional layer for friction

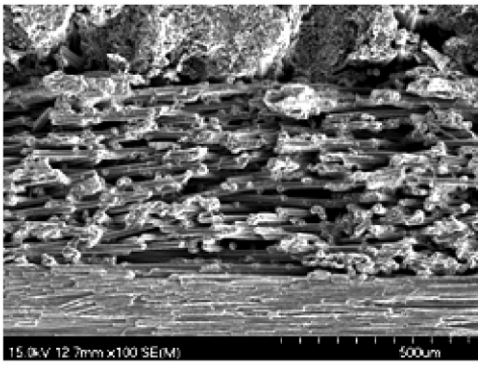

(c) mechanical function layer

Fig. 2. (a–c) The structure of 3D needled C/C porous composites with sandwich structure.

The fading ratio $D$ of the $\mu$ under wet condition, which represents the sensitivity of the $\mu$ to a humidity condition, is described as:

$$D = \left(1 - \frac{\mu_{wet}}{\mu_{dry}}\right) \times 100\% \quad (2)$$

where $\mu_{wet}$ is average $\mu$ under wet condition, and $\mu_{dry}$ average $\mu$ under dry condition.

The linear wear rate was determined by calculating the thickness difference. The friction test conditions to simulate the normal landing condition of the aircraft are listed in Table 1. The tests under each testing condition were repeated for 20 times.

## 3. Results and discussion

### 3.1. Phases analysis

The density and open porosity of the C/SiC brake materials with sandwich structure were 2.2 g/cm$^3$, and 4%, respectively.

Table 1
The parameters of friction testing condition.

| Testing condition | Inertia (kg m$^{-2}$) | Braking pressure (MPa) | Braking speed (m s$^{-1}$) |
|---|---|---|---|
| Dry | 0.235 | 0.9 | 25 |
| Wet | 0.235 | 0.9 | 25 |
| Static | – | 1.8 | – |

Table 2
The content of C, Si, and SiC in 3D needled C/SiC [7] and 3D needled C/SiC with sandwich structure brake materials.

| | 3D needled C/SiC | 3D needled C/SiC with sandwich structure | |
|---|---|---|---|
| | | Functional layer for friction | Mechanical functional layer |
| Content of C (wt%) | ~65 | ~49 | ~58 |
| Content of SiC (wt%) | ~27 | ~47 | ~40 |
| Content of Si (wt%) | ~8 | ~4 | ~2 |

The materials prepared by LSI process consisted of C, Si, and SiC [6]. The gravimetric analysis was employed to determine the content of C, Si, and SiC in the composites. Si was removed by dissolving the composite in a mixture of hydrofluoric and nitric acid ($HNO_3$:HF = 4:1) at 40 °C for 48 h, whereas the content of C was measured by burning it off at 700 °C for 20 h in air, so the content of residual SiC can be calculated. The content of C, Si, and SiC was shown in Table 2. The SiC content in the C/SiC sandwich materials is higher, compared to standard C/SiC material, whereas the Si content is lower.

### 3.2. Microstructure analysis

The SEM micrographs of the 3D needled C/SiC with sandwich structure were shown in Fig. 5. In Fig. 5, SiC and Si

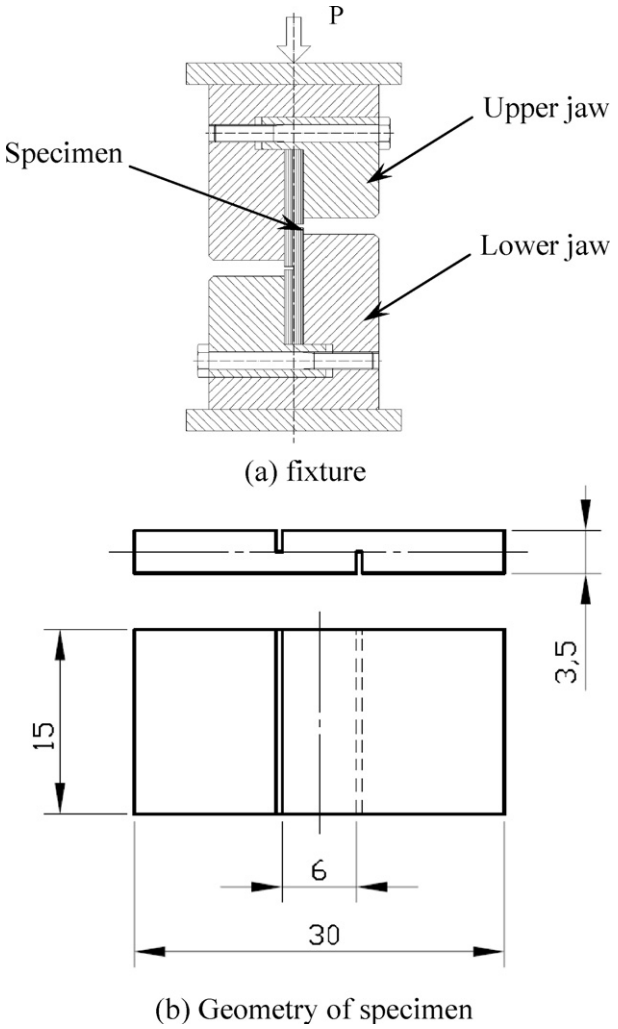


Fig. 3. (a and b) The fixture and the geometry of specimen for the inter-laminar shear strength test.

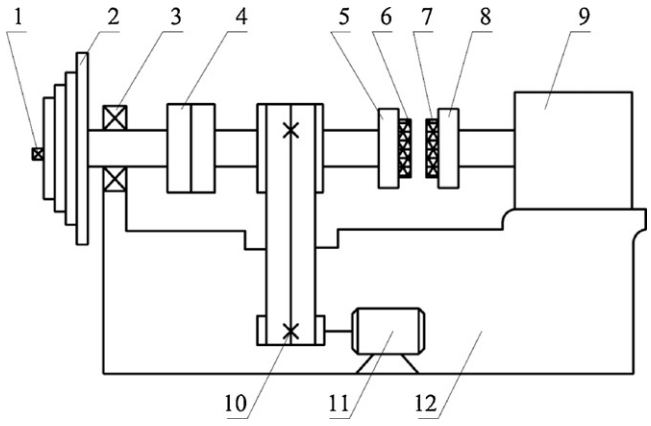


Fig. 4. Schematic diagram of the dynamometer: (1) clamp nut, (2) inertial wheel, (3) bearing, (4) clutch, (5) rotor holder, (6) rotor, (7) stator, (8) stator holder, (9) pressing cylinder, (10) strap, (11) motor, and (12) lathe-bed.

were distributed in grey regions, and pyrolytic carbon and carbon fibers were distributed in black regions. The BSE micrographs of the 3D needled C/SiC and friction layer for the 3D needled C/SiC with sandwich structure were shown in Fig. 6. In Fig. 6, SiC was distributed in grey regions, Si in white regions, and pyrolytic carbon and carbon fibers in black regions. Fig. 6(a) shows that the Si was presented clumped distribution in 3D needled C/SiC, and the content of Si was much. In Fig. 6(b) and (c), the Si was dispersed and the content was very little in the friction layer for the 3D needled C/SiC with sandwich structure. Figs. 5, 6(b) and (c) show that the distribution of the phases in the friction layer was homogeneous. In mechanical functional layer, SiC and Si were mostly distributed in the short fiber web layers, and local C/C composites [6] were kept in the non-woven fiber cloth layers. Local C/C protected the fibers from erosion by the molten silicon during the infiltration process. Therefore, the mechanical functional layers provided the materials high toughness and ensured against brittle failure.

The SEM micrograph of region between functional layer for friction and mechanical functional layer was shown in Fig. 7. It showed that no cracks and obvious interfaces were observed in the join region between functional layer for friction and mechanical functional layer. The inter-laminar shear strength of the join region was about $27 \pm 9$ MPa. And the typical fracture profiles were shown in Fig. 8. The needle fibers were pulled-out and sheared under the inter-laminar shear force (Fig. 8), which can strengthen the joining between functional layer for friction and mechanical functional layer.

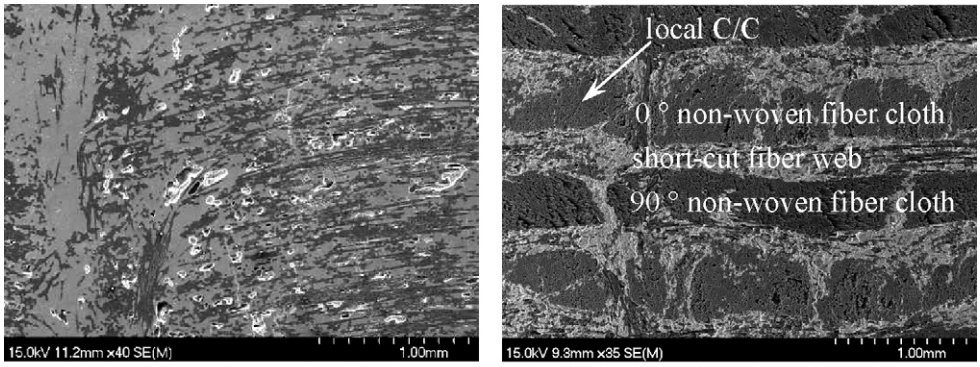


Fig. 5. (a and b) The SEM micrographs of the 3D needled C/SiC with sandwich structure.

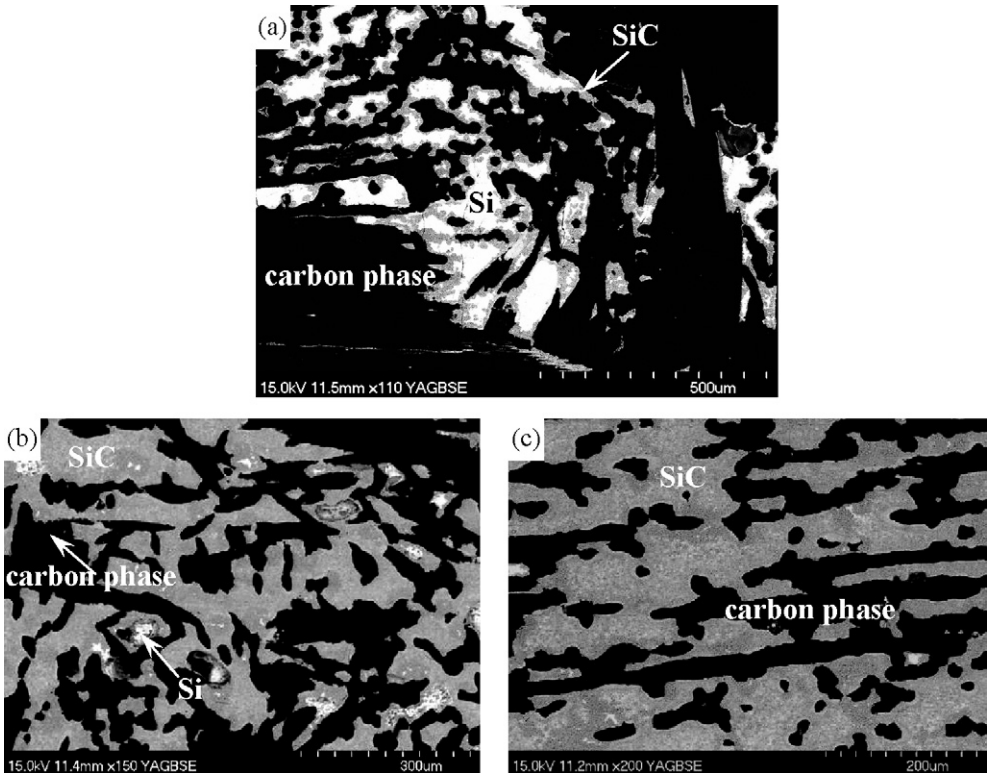


Fig. 6. The BSE micrographs of the 3D needled C/SiC and friction layer for the 3D needled C/SiC with sandwich structure: (a) 3D needled C/SiC, (b) parallel to the non-woven fiber cloth layers of friction layer for the 3D needled C/SiC with sandwich structure, (c) perpendicular to the non-woven fiber cloth layers of friction layer for the 3D needled C/SiC with sandwich structure.

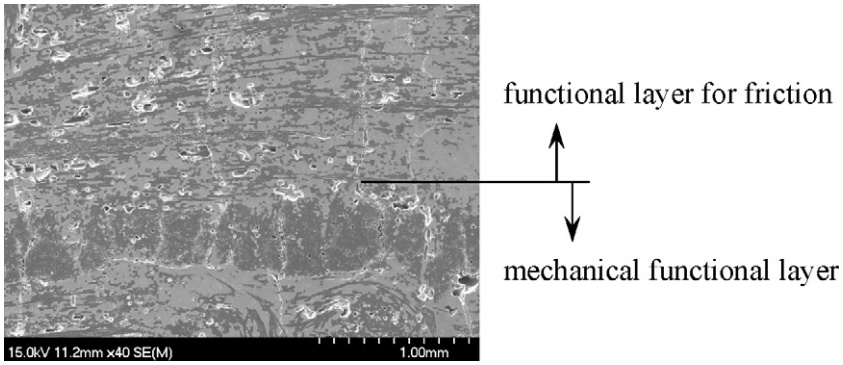


Fig. 7. The SEM micrograph of the region between functional layer for friction and mechanical functional layer.

### 3.3. Frictional properties

The frictional properties of the 3D needled C/SiC and C/SiC with sandwich structure are listed in Table 3. It indicated that frictional properties under wet condition of the C/SiC with sandwich structure had no fading, and was better than that of the 3D needled C/SiC. The static friction coefficient and linear wear rate of the C/SiC with sandwich structure were higher than that of the 3D needled C/SiC.

Under wet condition, the frictional properties of the carbon phase were prone to decline [13–15]. SiC phase was hard point on the friction surface, which tended to arouse ploughing action [5]. The ploughing action of the hard SiC was less affected by the humidity. The content of carbon was more, and the content

Table 3
The frictional properties of the 3D needled C/SiC and C/SiC with sandwich structure.

| | Friction coefficient | | Wet fading ratio, $D$/% | Static friction coefficient | Linear wear rate (μm/side cycle) |
|---|---|---|---|---|---|
| | Dry | Wet | | | |
| C/SiC with sandwich structure | 0.36 | 0.36 | 0 | 0.79–0.87 | 2.48 |
| 3D needled C/SiC | 0.38 | 0.34 | 10 | 0.45–0.68 | 2.16 |

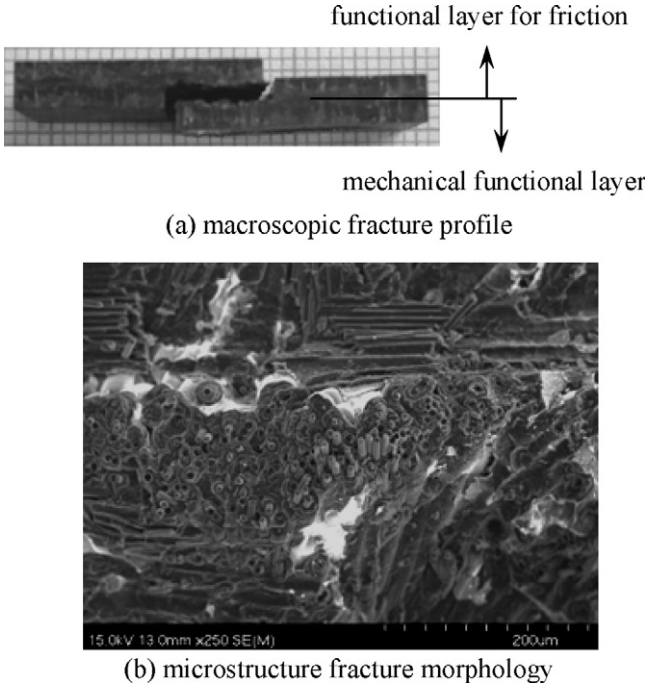


Fig. 8. (a and b) The inter-laminar shear fracture for sandwich C/SiC brake materials.

of SiC was less in the 3D needled C/SiC than those in C/SiC with sandwich structure, so that the frictional properties under wet condition of the C/SiC with sandwich structure was better than that of the 3D needled C/SiC. The interlayer force of graphitized carbon was low so that the graphitized carbon has good lubrication action, which led to low static friction coefficient and low wear rate for the graphitized carbon. The hard SiC was inclined to enhance the ploughing action, which resulted in the friction resistance and the wear rate increased. Therefore, the static friction coefficient and wear rate of the C/SiC with sandwich structure were higher than that of the 3D needled C/SiC at the normal landing condition of the aircraft.

Fig. 9 was the typical braking curves of 3D needled C/SiC and C/SiC with sandwich structure brake materials. It indicated

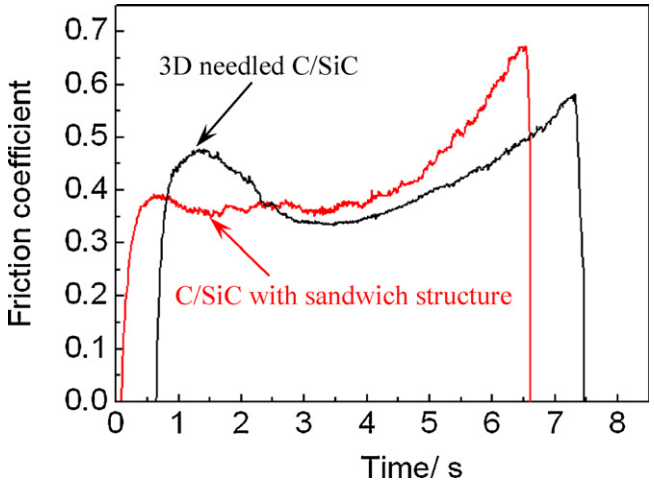


Fig. 9. Typical braking curves of 3D needled C/SiC and C/SiC with sandwich structure brake materials.

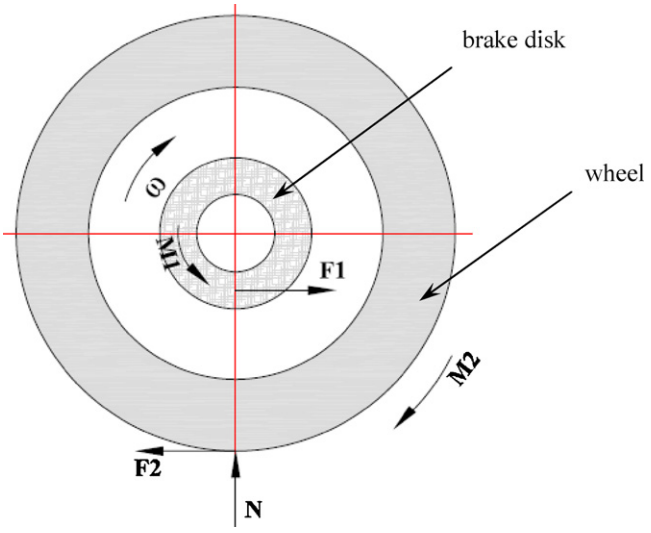


Fig. 10. Schematic illustration of forces on wheel and brake disk during aircraft braking. $M_1$ is braking moment, $F_1$ the friction force among brake disks, $M_2$ the traction moment of wheel, $F_2$ the friction force between wheel and land, $N$ the supported force on wheel by land, and $\omega$ is the rotational speed.

that the braking curve of C/SiC with sandwich structure was smoother than that of the 3D needled C/SiC, which revealed smooth braking for the C/SiC with sandwich structure.

A large amount of micro peaks on the friction surface are unavoidable. The micro peaks are generally referred to as asperities. At the prior stage of braking, only less asperities in the pair friction surface contacted and produced interaction, which led the temperature on the asperities very high and might be close to the melting point of the silicon. When the brake disks of the 3D needled C/SiC braked, the clumped silicon of the asperities in the friction surface would cause adhesive effect, which resulted in the friction coefficient abrupt change at the prior stage of braking. However, the silicon was little and dispersed in the friction layer of C/SiC with sandwich structure, and would not cause adhesive effect. Therefore, the braking curve of the C/SiC with sandwich structure was smooth.

The force analytical schematic illustration of brake disk and wheel during braking is shown in Fig. 10. The braking moment of brakes ($M_1$) and the traction moment of wheel ($M_2$) can be calculated from Eqs. (3) and (4).

$$M_1 = \frac{1}{2} PS\mu_1(R_1 + R_2)n \tag{3}$$

$$M_2 = N\mu_2 R_3 \tag{4}$$

where $P$ is the braking pressure, $S$ the area of the pressure acting, $\mu_1$ the friction coefficient of the braking materials, $R_1$ the inner radius of the friction surface, $R_2$ the outer radius of the friction surface, $n$ the number of the friction surface, $N$ the support force of the wheel by ground, $\mu_2$ the friction coefficient between wheel and ground, and $R_3$ is the radius of the wheel.

During the aircraft braking, the wheel would skid when $M_1$ was bigger than $M_2$, as a result of the wheel badly worn, even the tire cracked, and a catastrophic induced. Under anti-skid braking system, when the wheel would skid, the brake pressure can be lowered rapidly to decrease the $M_1$ and prevent the wheel

skidding. After the brake pressure was lowered by the anti-skid braking system, the wheel rolled normally, and then the braking system would increase the brake pressure to achieve the effective braking. During the braking system decompressing, the braking system did not brake almost which resulted in lower brake efficiency.

The braking curve of C/SiC with sandwich structure exhibited an upended trapezium shape, which was consistent with the landing response of the aircraft with anti-skid braking system. At the prior stage of braking, the braking speed was high so that the aircraft could generate lift, to reduce the N, namely, to reduce the $M_2$. When the braking speed was high, the needed $M_1$ was smaller to prevent the wheel skidding. With the braking proceeding, the speed of the aircraft was reduced continuously which led to the lift force decreased, the N and $M_2$ increased continuously, and then the needed $M_1$ increased continuously. The friction coefficient of the brake materials matched the landing response of aircraft with anti-skid braking system, which would lead to a higher brake efficiency.

## 4. Conclusions

(1) The C/SiC brake materials with sandwich structure were prepared by a combined process of CVI, SI and LSI. The materials were composed of inner mechanical functional layer, and two outer frictional functional layers. The density and open porosity of the materials were 2.2 g/cm$^3$, and 4%, respectively. The SiC was more in C/SiC with sandwich structure than that in 3D needled C/SiC, and the Si was less than that in 3D needled C/SiC.

(2) The distribution of the phases in the functional layer for friction of C/SiC with sandwich structure was homogeneous, and the Si was little in the functional layer for friction. The join region between functional layer for friction and mechanical functional layer has not cracks, and obvious interface. The inter-laminar shear strength of the join region was about $27 \pm 9$ MPa, which revealed the joining reliable.

(3) The frictional properties under wet condition of the C/SiC with sandwich structure were no fading, and were better than that of the 3D needled C/SiC. The static friction coefficient and linear wear rate of the C/SiC with sandwich structure were higher than that of the 3D needled C/SiC. The C/SiC with sandwich structure brake materials would have higher brake efficiency.

## Acknowledgements

The authors acknowledge the project supported by the Research Fund of State Key Laboratory of Solidification Processing (NWPU), China (Grant no. 46-QP-2009), and Program for Changjiang Scholars and Innovative Research Team in University.

## References

[1] S. Vaidyaraman, M. Purdy, T. Walker, S. Horst, C/SiC materials evaluation for aircraft brake applications, in: W. Krenkel, R. Naslain, H. Schneider (Eds.), High Temperature Ceramic Matrix Composites, Wiley-VCH, New York, 2001, pp. 802–808.
[2] W. Krenkel, T. Henke, Design of high performance CMC brake disks, Key Eng. Mater. 164–165 (1999) 421–424.
[3] W. Krenkel, C/C–SiC composites for hot structures and advanced friction systems, Ceram. Eng. Sci. Proc. 24 (2003) 583–592.
[4] A. Mühlratzer, M. Leuchs, Application of non-oxide CMCs, in: W. Krenkel, R. Naslain, H. Schneider (Eds.), High Temperature Ceramic Matrix Composites, Wiley-VCH, New York, 2001, pp. 288–298.
[5] S. Fan, L. Zhang, Y. Xu, L. Cheng, G. Tian, S. Ke, et al., Microstructure and tribological properties of advanced carbon/silicon carbide aircraft brake materials, Compos. Sci. Technol. 68 (2008) 3002–3009.
[6] S. Fan, L. Zhang, Y. Xu, L. Cheng, J. Lou, J. Zhang, et al., Microstructure and properties of 3D needle-punched carbon/silicon carbide brake materials, Compos. Sci. Technol. 67 (2007) 2390–2398.
[7] http://en.wikipedia.org/wiki/Disc_brake.
[8] W. Krenkel, CMC materials for high performance brakes, in: W. Krenkel, R. Naslain, H. Schneider (Eds.), High Temperature Ceramic Matrix Composites, Wiley-VCH, New York, 2001, pp. 769–775.
[9] Z.S. Pak, Cf/SiC/C composites for frictional application, in: W. Krenkel, R. Naslain, H. Schneider (Eds.), High Temperature Ceramic Matrix Composites, Wiley-VCH, New York, 2001, pp. 820–825.
[10] W. Krenkel, F. Berndt, C/C–SiC composites for space applications and advanced friction systems, Mater. Sci. Eng. A 412 (2005) 177–181.
[11] S. Fan, L. Zhang, L. Cheng, G. Tian, S. Yang, Effect of braking pressure and braking speed on the tribological properties of C/SiC aircraft brake materials, Compos. Sci. Technol. 70 (2010) 959–965.
[12] S. Fan, L. Zhang, L. Cheng, J. Zhang, S. Yang, H. Liu, Wear mechanisms of wear mechanisms of the C/SiC brake materials, Tribol. Int. 44 (2011) 25–28.
[13] J.D. Chen, J.H. Chern Lin, C.P. Ju, Effect of humidity on the frictional behavior of carbon–carbon composites, Wear 193 (1996) 38–47.
[14] B.K. Yen, Influence of water vapor and oxygen on the tribology of carbon materials with sp2 valence configuration, Wear 192 (1996) 208–215.
[15] C. Blanco, J. Bermejo, H. Marsh, R. Menendez, Chemical and physical properties of carbon as related to brake performance, Wear 213 (1997) 1–12.